Molecules **2012**, *17*, 10801-10815; doi:10.3390/molecules170910801

OPEN ACCESS

molecules

ISSN 1420-3049

www.mdpi.com/journal/molecules

Article

Photoelectrode Characteristics of Partially Hydrolyzed Aluminum Phthalocyanine Chloride/Fullerene C_{60} Composite Nanoparticles Working in a Water Phase

Shuai Zhang [1,2], Toshiyuki Abe [3], Tomokazu Iyoda [1] and Keiji Nagai [1,*]

[1] Chemical Resources Laboratory, Division of Integrated Molecular Engineering, Tokyo Institute of Technology, Yokohama 226-8503, Japan; E-Mails: shuaizhang@cczu.edu.cn (S.Z.); iyoda.t.aa@m.titech.ac.jp (T.I.)

[2] Center for Low-Dimensional Materials, Micro-Nano Devices and System, Changzhou University, Changzhou 213164, Jiangsu, China

[3] Department of Frontier Materials Chemistry, Graduate School of Science and Technology, Hirosaki University, 3 Bunkyo-cho, Hirosaki, Aomori 036-8561, Japan; E-Mail: tabe@cc.hirosaki-u.ac.jp

* Author to whom correspondence should be addressed; E-Mail: nagai.k.ae@m.titech.ac.jp; Tel.: +81-45-924-5266; Fax: +81-45-924-5247.

Received: 25 July 2012; in revised form: 28 August 2012 / Accepted: 5 September 2012 / Published: 10 September 2012

Abstract: Photoelectrochemical measurements were used to study the photoelectrode characteristics of composite nanoparticles composed of fullerene C_{60} and partially hydrolyzed aluminum phthalocyanine chloride (AlPc). In cyclic voltammetry measurements, the electrodes coated with the composite nanoparticles were found to have photoanodic [electron donor: 2-mercaptoethanol (ME)] and photocathodic (electron acceptor: O_2) characteristics similar to those of the vapor-deposited p/n junction electrode. Their photoanodic features were further investigated with respect to the transient photocurrent response to light irradiation and the dependence on ME concentration (under potentiostatic conditions), from which it was noted that there was a decrease in the initial spiky photocathodic current and saturation of the steady-state photoanodic current at a higher ME concentration. Thus, the reaction kinetics was probably dominated by charge transport process. Moreover, external and internal quantum efficiency spectrum measurements indicated that the composite nanoparticles responded to the full spectrum of visible light (<880 nm) for both the photoanodic and photocathodic current. The present research will assist comprehension of photocatalytic behavior of the composite nanoparticles.

Keywords: organophotocatalyst; fullerene; phthalocyanine; photoelectrochemistry

1. Introduction

Phthalocyanines (Pcs) constitute a remarkably versatile and robust class of compounds with diverse technological applications. For instance, metallophthalocyanines, in which the two hydrogen atoms of the central cavity can be replaced by more than 70 metals [1], have been used as efficient biomimetic catalysts for oxidation, reduction, and other reactions of organic compounds [2–6]. Besides, due to Pcs' thermal and chemical stability, intense absorption in the red/near-infrared (IR) region of the solar spectrum, quite high fluorescence quantum yields, and capability to act as an electron donor for the acceptor moiety, they become valuable building blocks in organic photovoltaic devices [7–13], dye sensitized solar cells [14–20], photocatalysts [21–28], laser ablation control [29,30], and so on. In the application of photocatalysts, Pcs may act as photosensitizers to extend the absorption edge of some semiconductors with large band gap [21–23] through an intercomponent electron transfer. Otherwise, Abe and co-workers recently applied Pcs to organic photoelectrocatalysts with p/n junction and achieved water splitting under visible light and a small bias [24,25]. Nagai and co-workers combined the p/n layer with the absorbent Nafion and achieved photodegradation of trimethylamine to CO_2 without bias [26]. Based on the report about the organophotocatalysts, we further developed nanoparticulate organic photocatalysts composed of C_{60} and partially hydrolyzed aluminum phthalocyanine chloride (AlPc) [27,28]. The composite exhibited photocatalytic superiority over single component nanoparticles for photodegradation of various organic substrates to CO_2 without absorbent or bias, and its CO_2 action spectrum for decomposition of 2-mercaptoethanol (ME) covered almost full spectrum of visible light [28]. However, the role of the composite in the photocatalysis was still unclear.

Photoelectrochemistry is one of the most promising methods for investigating and establishing photoenergy conversion systems, in which the photoelectrochemical water splitting system of a TiO_2 electrode [31] as well as the dye-sensitized photovoltaic cell of a Ru complex absorbed on TiO_2 electrode [32] are typical examples. It has also been used to study photo-induced oxidation and reduction reactions separately for the organic photoelectrocatalysts [24,25,33–35] or photocatalysts [26] with p/n junction. In the present research, the photoanodic and photocathodic characteristics of the ME oxidation and the reduction involving O_2, respectively for the AlPc/C_{60} composite nanoparticles were investigated by the method. The research will offer benefit for comprehension of photocatalytic behavior of the composite nanoparticles.

2. Results and Discussion

2.1. Comparison of Photoanodic Characteristics for Electrodes Composed of Different Nanoparticles

The photoanodic characteristics of nanoparticle electrodes were first investigated by means of cyclic voltammetry. In our previous research [27], a comparison of the photoanodic threshold potential values between the nanoparticles and vapor-deposited films demonstrated that the composite nanoparticles have photoelectrochemical characteristics similar to the C_{60}/AlPcCl layer, where

trimethylamine (TMA) was used as the electron donor. In this study, the nanoparticle electrodes exhibit the same threshold potential values as those in the previous research: −0.2 V, ~+0.4 V (anodic current), and −0.2 V for the C_{60}, AlPc, and composite nanoparticles, respectively (obtained from Figure 1), although the electron donor was changed from TMA to ME. Furthermore, single component nanoparticles exhibit a small net photoanodic current and only an anodic dark current for the C_{60} (Figure 1a) and AlPc nanoparticles (Figure 1b), respectively, as a result of the semiconductor/liquid interface of a Schottky junction [36]. The composite nanoparticles (Figure 1c) show a superior net photoanodic current as compared to that of either C_{60} or AlPc. The results demonstrate that the photoanodic characteristics of the nanoparticles are based on the semiconducting characters of the corresponding p- or n-type semiconductor layer for the single-component nanoparticles and the formation of p/n junction for the composite nanoparticles.

Figure 1. Cyclic voltammograms of particle films of (**a**) C_{60}; (**b**) AlPc; and (**c**) composite on ITO: solid line, under illumination; dashed line, in the dark. The electrolyte solution: 2×10^{-3} mol/L 2-mercaptoethanol (PH ~ 10) in an Ar atmosphere; Scan rate: 20 mV/s; light intensity: 100 mW/cm^2. The composite's loading mole ratio of AlPcCl to C_{60} was 5:4.

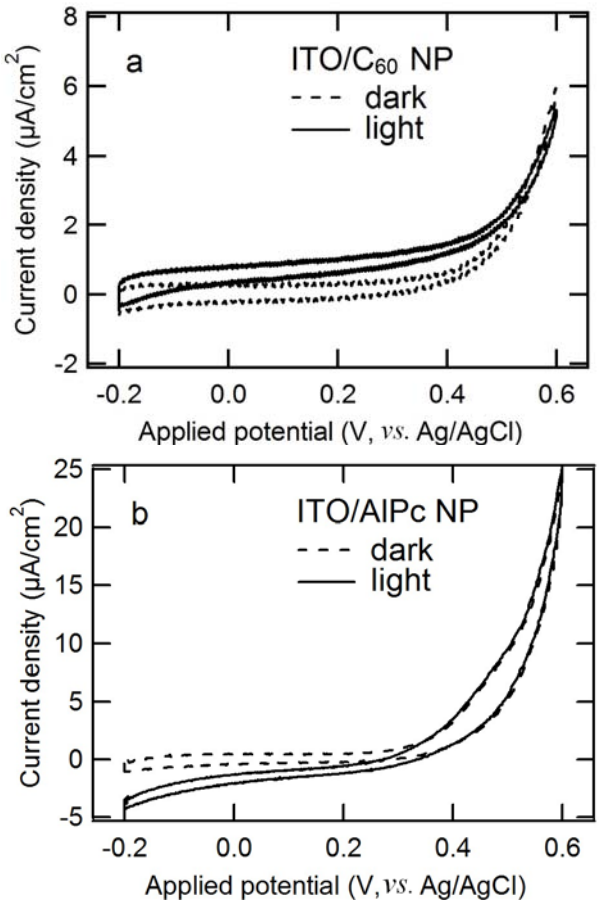

Figure 1. *Cont.*

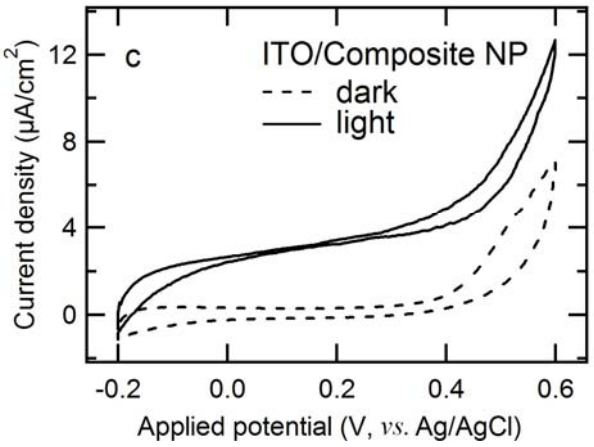

2.2. Kinetic Characteristics of Photoanode Composed of Composite Nanoparticles

2.2.1. Transient Photoanodic Current Generated at ITO/Composite Nanaoparticles

To investigate the kinetic characteristics of ME oxidation at the composite nanoparticle/water interface, measurements of the photoelectrochemical response to light irradiation were carried out. Figure 2a shows a typical photoelectrochemical response of the electrode (ITO/composite nanoparticles) immediately after irradiating a white light (intensity: 100 mW/cm^2) under potentiostatic conditions. Initially, a spiky photocurrent (J_{in}) is observed, which then attains a steady-state (J_s represents the steady-state photocurrent). However, the sign of the photocurrent spike (cathodic) is the opposite of that of the steady-state anodic photocurrent, which is different from the reported electrode of ITO/C_{60}/H2Pc [36]. The observed spiky photocathodic current is probably composed of two contributions: a photoanodic contribution due to ME oxidation [36] and a photocathodic contribution [37] due to several possible reasons (*vide post*). The former increases with the ME concentration, while the later remains constant, so the resultant photocathodic current decreases with the ME concentration (*vide post*, Figure 3a, J_{in}). The origin of the photocathodic contribution is still unclear, but several factors are suggested. The first is the formation of O_2-bridged metal Pc dimer [38], for which the photocathodic contribution may be the result of O_2 reduction through electron transfer from photoexcited AlPc to oxygen. Second, it has been reported that Pcs may undergo photo-oxidation involving singlet oxygen addition to the macrocyclic rings [39], which can be achieved in the particle preparation process of the present research. The oxidized Pcs may be also reduced by electron transfer from photoexcited AlPc, and hence the photocathodic contribution is generated. These two hypotheses are consistent with the wavelength dependency of the photocathodic spike (Figure 2b,c): the unusual spike disappears at the wavelength (*i.e.*, 500 nm) where AlPc has little absorbance, whereas it appears at 700 nm where AlPc has remarkable absorbance, but they cannot account for the photoanodic spike observed immediately after blocking light (Figure 2a,c), which indicates the existence of reversible reactions. Further considering that the absolute value of the photocathodic spike is larger than that of the photoanodic one (Figure 2a,c), it is found that the reactions corresponding to the photocathodic spike are partially reversible. Therefore, the other two possibilities are also proposed: the rearrangement of the electrical double layer in response to photogenerated charge carriers and the presence of localized midgap states

in AlPc. They were also considered as the reasons for the unusual photocathodic and photoanoic spikes for the nickel hydroxide thin-film electrode after irradiating and blocking light, respectively [37].

Figure 2. Time course of photocurrent generated by ITO/composite electrode: (**a**) The electrolyte contained 0.5 mmol/L 2-mercaptoethanol (PH ~ 10) in an Ar atmosphere; applied potential = +0.3 V (*vs*. Ag/AgCl); light intensity = 100 mW/cm^2. (**b**) and (**c**) The electrolyte contained 2 mmol/L 2-mercaptoethanol (PH~10) in an Ar atmosphere; Applied potential = +0.3 V (*vs*. Ag/AgCl); the number of incident photon was adjusted to 3.5×10^{13} cm^{-2}s^{-1} at different wavelength. The composite's loading mole ratio of AlPcCl to C_{60} was 5:4.

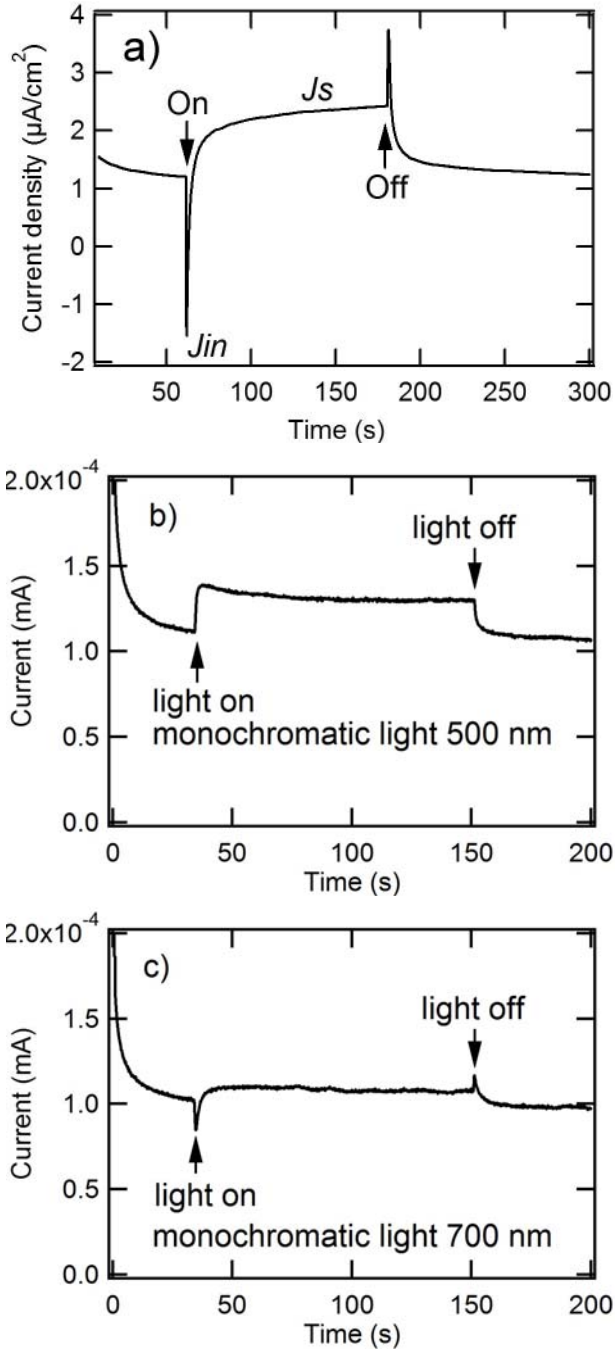

2.2.2. Dependence of Photocurrent on ME Concentration

Figure 3a shows that the steady-state anodic photocurrent increases, whereas the spiky photocathodic one decreases with the ME concentration. Both the photocurrents deviate from the linear relationship (Figure 3a). If the steady-state anodic photocurrent increased linearly with the ME concentration, it would indicate that the electrode kinetics were completely dominated by a mass transport of ME (electron transport from ME to the electrode took place efficiently, and the mass transport process was the rate-determining step). However, in the present system, this is not the case. The results show that the photocurrent deviates from the linear relationship even in the low concentration region (*i.e.*, order of mmol/L), which probably indicates that the electrode reaction kinetics are dominated by an electrochemical process (*i.e.*, charge transport between ME and AlPc) [36]. The steady-state photocurrent (J_s) may be analyzed to assume a Langmuir adsorption prior to the rate-limiting charge transfer step, where only the adsorbed ME with a surface concentration (Γ) is photoelectrochemically oxidized and the reaction products are quickly desorbed from the semiconductor surface [36,40]. Therefore the following two equations are valid:

$$J / nF = k_f[h^*]_0\Gamma \quad (1)$$

$$d\Gamma / dt = k(\Gamma_{max} - \Gamma)C_R - k'\Gamma - k_f[h^*]_0\Gamma \quad (2)$$

where n, the number of electrons transferred to a thiol molecular; F, Faraday's constant; k_f, rate constant of the electrochemical reaction; $[h^*]_0$, the surface concentration of the holes; k, the rate constant of adsorption; k', the rate constant of desorption; C_R, the thiol concentration in the electrolyte; and Γ_{max}, the postulated maximum coverage when all available sites are occupied.

In the steady-state, from $d\Gamma / dt = 0$, Equation (3) is derived. Furthermore, Equation (4) is obtained by inserting J from Equation (1) into Equation (3):

$$k(\Gamma_{max} - \Gamma)C_R = k'\Gamma + k_f[h^*]_0\Gamma \quad (3)$$

$$C_R / J_s = C_R / J_{max} + \{(k' / k) + (k_f[h^*]_0 / k)\} / J_{max} \quad (4)$$

where J_{max} is the postulated photocurrent from Γ_{max}. The plot of C_R/J_s *vs*. C_R (Figure 3b) shows a linear relationship that is constant with Equation (4). From the slope of the line, J_{max} was calculated to be 6.3 μA/cm^2. The value is 100 times smaller than that of the reported organic electrode [36] which reached 6.3 × 10^2 μA/cm^2, probably due to the poor electron injection into the ITO electrode and random orientations of the composite nanoparticles to the base electrode [27].

2.3. EQE and IQE Spectra for Steady-State Photoanodic Current

In order to determine the origin of the photoanodic current, its EQE and IQE spectra were measured (Figure 4). The resulting EQE spectrum covers the full spectrum of visible light, even reaching 860 nm, which is consistent with the composite's absorption edge. Moreover, it almost corresponds with the absorption spectrum, which demonstrates that the present photocurrent generation is induced by the light absorption of both C_{60} and AlPc in the composite. A similar phenomenon was observed for the vapor-deposited organic electrode of C_{60}/H_2Pc [36,41]. The photoanodic current (Figure 1c) is mainly derived from the ME oxidation by holes in AlPc that are generated through the migration of the

excitation energy of C_{60} and/or AlPc and the following charge separation at p/n junction, by taking into account the charge separation characteristics of the composite (because of its photocurrent superiority, as shown in Figure 1). The IQE values are absorbance-dependent: high absorbance mainly gives small IQE values, and low absorbance gives large IQE values. It can be interpreted according to an optical filter effect by AlPc itself and the higher probability of exciton diffusion to the p/n interface in the case of low absorbance [27] as shown in Figure 5. Although the IQE values are lower around the wavelength of 800 nm where AlPc has large absorbance, the dye still has important role for the composite: The AlPc material can form a heterojunction with C_{60} in the composite and enhance charge separation. Hence, the net photoanodic current (Figure 1) of the composite is superior to that of the single component C_{60} or AlPc. In addition, the presence of AlPc also increases light harvesting compared to the single component C_{60}.

Figure 3. (**a**) The dependencies of the initial spiky photocurrent (J_{in}, ■,) as well as steady-state photocurrent (J_s, ▲,) on the ME concentration. (**b**) The plots of the ME concentration in the electrolyte (C_R) / the steady-state photocurrent (J_s) *vs*. C_R. Applied potential = +0.3 V (*vs*. Ag/AgCl); light intensity = 100 mW/cm^2; measured in an Ar atmosphere. The composite's loading mole ratio of AlPcCl to C_{60} was 5:4.

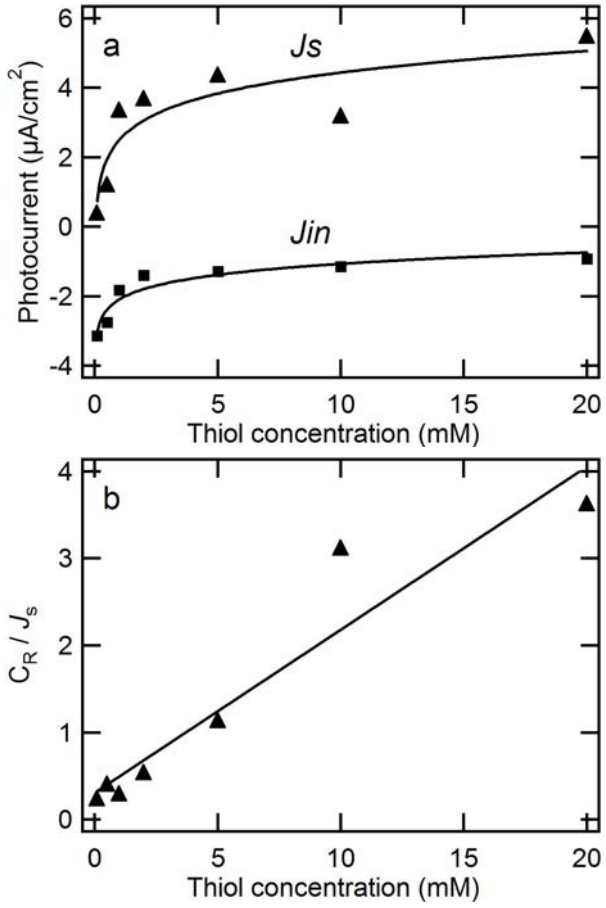

Figure 4. Steady-state EQE (●) and IQE (■) spectra for photoanodic current generated at ITO/composite nanoparticles and absorption spectrum of the electrode employed (solid line). The number of incident photon was adjusted to 3.5×10^{13} $cm^{-2}s^{-1}$ at each wavelength. ME concentration, 10 mM (pH, 10); Applied potential, +0.3 V; measured in an Ar atmosphere. The composite's loading mole ratio of AlPcCl to C_{60} was 5:4.

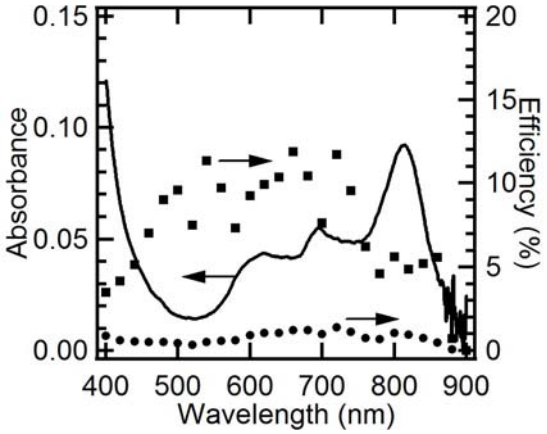

Figure 5. Schematic representation of the correlation between absorption coefficient and exciton diffusion length. The p-type semiconductor has large absorption coefficient at the frequency ν′, and small coefficient at the ν.

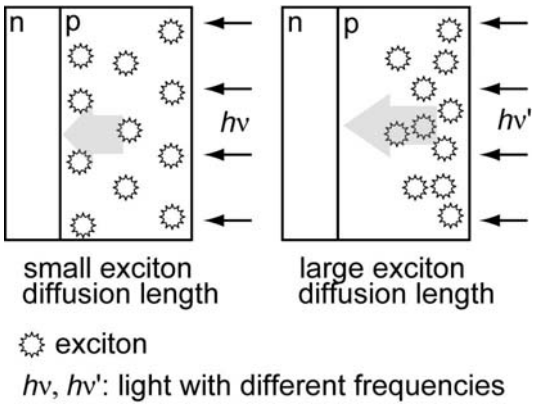

2.4. Comparison of Photocathodic Characteristics for Vapor-Deposited Electrodes

Photoinduced oxidation and reduction exist simultaneously in photocatalytic reactions. The former has been studied for composite nanoparticles in terms of the photoanodic characteristics (Figures 1–4). To further understand the composite nanoparticles' photocatalytic mechanism, photoelectrochemical methods were also used to study their photocathodic properties relating to O_2 reduction. First of all, as a reference for the nanoparticles, vapor-deposited organic semiconductor electrodes composed of C_{60} and/or AlPcCl were studied. Figure S1 shows the photocathodic currents for all the samples, and their threshold potential values are ~+0.14 V, ~+0.33 V, ~+0.33 V, and ~+0.4 V for ITO/C_{60}, ITO/AlPcCl, ITO/C_{60}/AlPcCl, and ITO/AlPcCl/C_{60}, respectively. The photocathodic currents of the ITO/C_{60}/AlPcCl and ITO/C_{60} electrodes showe saturation at potentials of about 0.3–0.0 V and 0.2–0.0 V, respectively, while the ITO/AlPcCl/C_{60} and ITO/AlPcCl electrodes showe notable photocathodic current increase at potentials of about 0.4–0.0 V and 0.3–0.0 V, respectively, which agrees with the scheme (Figure S2).

The larger net photocathodic current for ITO/AlPcCl/C_{60} compared to that for ITO/C_{60} implies the efficient reduction involving oxygen by electrons in C_{60} generated at the AlPcCl/C_{60} interface.

2.5. Comparison of Photocathodic Characteristics for Electrodes Composed of Different Nanoparticles

In the nanoparticle case, Figure 6 also shows the photocathodic currents for all of the samples. The photocathodic current is caused by the reduction involving oxygen because it almost disappears after Ar was bubbled into the electrolyte (Figure S3). The threshold potential values are ~+0.10 V, ~+0.33 V, and ~+0.33 V for the C_{60}, AlPc, and composite nanoparticles, respectively. This shows the similarity between the nanoparticles and the corresponding vapor-deposited electrode (Figure S1), demonstrating that the photocathodic characteristics of the nanoparticles are also based on the semiconducting characteristics of the p, n, or p/n layer. The threshold potential value of the composite nanoparticles (Figure 6c) is a little less positive than that of the p/n layer (Figure S1d) as a result of random orientations of the composite nanoparticles relative to the ITO electrode surface [27]. The observed photocathodic current indicates that the consumption of photoexcited electrons in the composite may be through a multielectron reduction of O_2 according to the conduction band level of C_{60} [42].

Figure 6. Cyclic voltammograms of particle films of (**a**) C_{60}, (**b**) AlPc, and (**c**) composite on ITO: solid line, under illumination; dashed line, in the dark. The electrolyte solution contained 0.1 M KNO_3 in an air atmosphere; Scan rate: 20 mV/s; light intensity: 100 mW/cm^2. The composite's loading mole ratio of AlPcCl to C_{60} was 5:4.

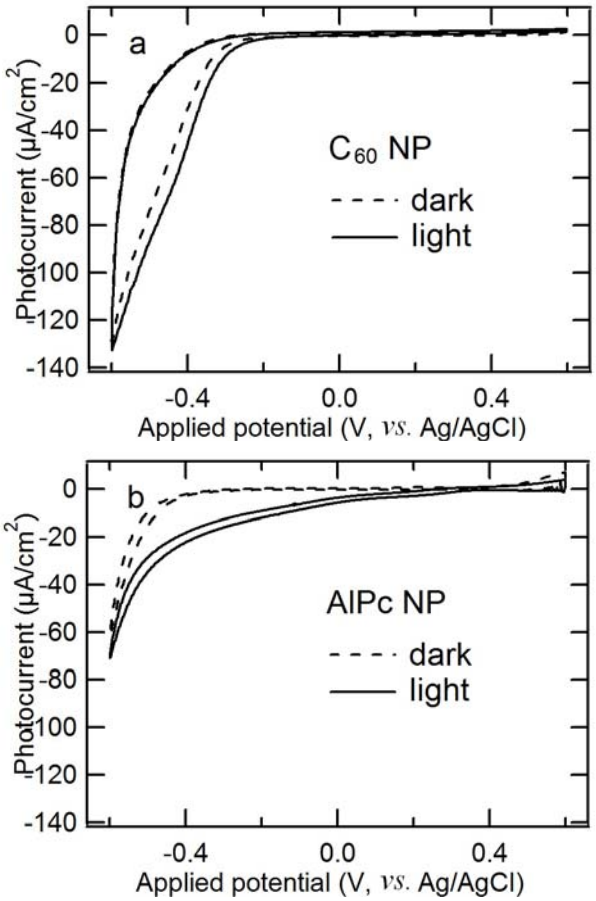

Figure 6. *Cont.*

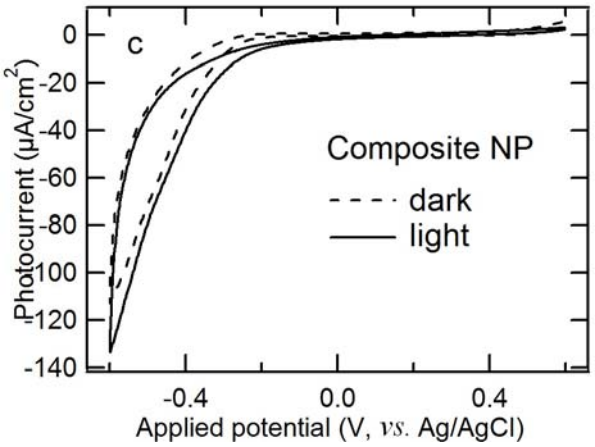

2.6. EQE and IQE Spectra for Steady-State Photocathodic Current

Figure 7 shows the EQE and IQE spectra of the photocathodic current involving oxygen for the composite particles. Similar to the spectra of the photoanodic current in Figure 4, it is found that the EQE spectrum in Figure 7 is almost consistent with the absorption spectrum and covers the full spectrum of visible light, indicating that the present photocathodic current is generated by the light absorption of both C_{60} and AlPc in the composite. The photocathodic current may be derived from the reduction involving O_2 by electrons that are generated through the migration of the excitation energy of C_{60} and/or AlPc and the following charge separation at Schottky or p/n junction, by taking into account the photocathodic characteristics of the different nanoparticles (Figure 6). The highest IQE value reaches 8%, and the values are also absorbance-dependent as discussed in the part of photoanodic characteristics.

Figure 7. Steady-state EQE (●) and IQE (■) spectra for photocathodic current generated at ITO/composite nanoparticles and absorption spectrum of the electrode employed (solid line). The number of incident photon was adjusted to 3.5×10^{13} $cm^{-2}s^{-1}$ at each wavelength. The electrolyte contained 0.1 M KNO_3 in an air atmosphere; Applied potential, +0.3 V. The composite's loading mole ratio of AlPcCl to C_{60} was 5:4.

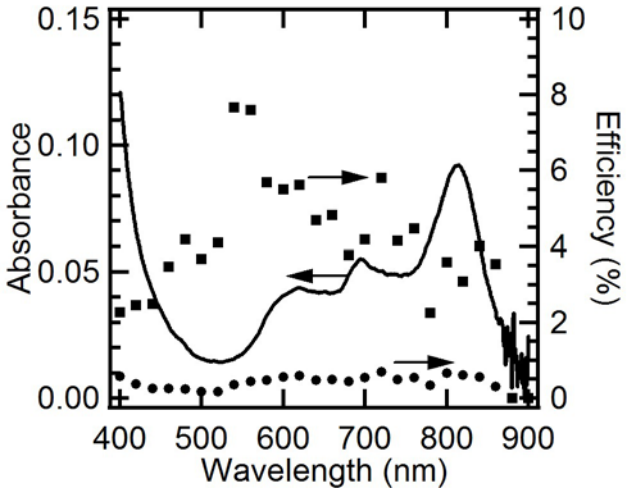

3. Experimental

3.1. Materials

Fullerene C_{60} (99%) was obtained from Tokyo Chemical Industry Co., Ltd. (TCI), and was used as received. Aluminum phthalocyanine chloride (AlPcCl, TCI) was purified twice by sublimation prior to its use. An indium tin oxide-coated (ITO-coated) glass plate (resistance: 8 Ω cm^{-2}; transmittance: >85%; thickness: 174 nm) was commercially obtained from Asahi Glass Co., Ltd., and was washed using sonication in water containing detergent, pure water, acetone, and ethanol, in that sequence. The ITO plate was dried in air before use. All the other solvents and chemicals were of reagent-grade quality, purchased commercially, and used without further purification.

3.2. Particle Synthesis and Electrode Preparation

Organic semiconductor nanoparticles composed of AlPc and/or C_{60} were prepared according to our previous research [27,28]. The loading mole ratio of AlPcCl to C_{60} was controlled to be 5:4. Working electrodes were prepared by simply casting particle suspensions after filtration on an ITO glass surface and drying at room temperature. For instance, 0.15 mL of 0.1 mg/mL suspension was cast on an ITO electrode with an effective area of 1 cm^2.

3.3. Photoelectrochemical Measurements

All the photoelectrochemical measurements were carried out in a standard three-electrode system, which was equipped with a modified ITO working electrode, a Pt wire counter electrode, and a Ag/AgCl (in saturated KCl electrolyte) reference electrode, using an electrochemical workstation (Hokuto Denko HSV-100). The working electrode was placed in contact with different electrolytes in an Ar or air atmosphere. A halogen lamp was used as the light source, and light was illuminated on the working electrode from the ITO side. The light intensity of 100 mW/cm^2 was monitored and corrected using an optical power meter (3A-SH, Ophir, Ltd.).

The external quantum efficiency (EQE) and internal quantum efficiency (IQE) spectra for the photoanodic and photocathodic current were measured using a halogen lamp (150 W) as the light source in combination with a monochromator (SG-100, Kohken Co., Ltd.). The incident photon number intensity was adjusted to 3.5×10^{13} $cm^{-2}s^{-1}$ at each wavelength and was monitored using the power meter. In the experiment, an electrolyte containing 1×10^{-2} mol/L 2-mercaptoethanol (ME) (pH ~ 10) in an Ar atmosphere or 0.1 mol/L KNO3 in an air atmosphere was used. The EQE and IQE were calculated using Equations (1) and (2), respectively:

$$\text{EQE (\%)} = [(I/e)/(W/\varepsilon)] \times 100 \quad (5)$$

$$\text{IQE (\%)} = \{[I/e]/[W \times (1 - 10^{-A})/\varepsilon]\} \times 100 \quad (6)$$

where I (A/cm^2) is the photocurrent density; e (C) is the elementary electric charge; W (W/cm^2) is the light intensity; ε is the photon energy (J); and A is the absorbance of the composite nanoparticles on the electrode.

4. Conclusions

We have investigated the photoelectrode characteristics of a nanoparticulate organic semiconductor composite. The electrode coated with the composite nanoparticles was found to carry out photo-induced oxidation of ME or reduction involving O_2, and p/n junction of the composite nanoparticles further enhances the photoanodic current. EQE and IQE spectra of the electrode covers full spectrum of visible light (<880 nm) for the steady-state photoanodic and photocathodic current under potentiostatic conditions. The results reported herein may benefit comprehension of the photocatalytic behavior of composite nanoparticles.

Supplementary Materials

Supplementary materials can be accessed at: http://www.mdpi.com/1420-3049/17/9/10801/s1.

Acknowledgments

This research was supported by the New Energy and Industrial Technology Development Organization, Tokyo Ohka Foundation, Japan, and a Grant-in-Aid for Scientific Research from MEXT, Japan (Grant 22350099 and 24655169).

References

1. Bottari, G.; de la Torre, G.; Guldi, D.M.; Torres, T. Covalent and noncovalent phthalocyanine-carbon nanostructure systems: Synthesis, photoinduced electron transfer, and application to molecular photovoltaics. *Chem. Rev.* **2010**, *110*, 6768–6816.
2. Shaabani, A.; Farhangi, E.; Rahmati, A. Aerobic oxidation of alkyl arenes and alcohols using cobalt(II) phthalocyanine as a catalyst in 1-buty-3-methyl-imidazolium bromide. *Appl. Catal. A-Gen.* **2008**, *338*, 14–19.
3. Kotronarou, A.; Hoffmann, M.R. Catalytic autoxidation of hydrogen sulfide in wastewater. *Environ. Sci. Technol*. **1991**, *25*, 1153–1160.
4. Joseph, J.K.; Jain, S.L.; Sain, B. Covalently anchored polymer immobilized Co(II) phthalocyanine as efficient catalyst for oxidation of mercaptans using molecular oxygen as oxidant. *Ind. Eng. Chem. Res.* **2010**, *49*, 6674–6677.
5. Kasuga, K.; Tsuboi, K.; Handa, M.; Sugimori, T.; Sogabe, K. Oxygen-oxygenation of cyclohexene catalyzed by manganese(III), iron(III) and cobalt(II) complexed of *tetra-tert*-butylphthalocyanine in the presence of iso-butyraldehyde. Inorg. *Chem. Commun.* **1999**, *2*, 507–509.
6. Parton, R.F.; Neys, P.E.; Jacobs, P.A.; Sosa, R.C.; Rouxhet, P.G. Iron-phthalocyanine immobilized on active carbon black: A selective catalyst for alkane oxidation. *J. Catal.* **1996**, *164*, 341–346.
7. Tang, C.W. Two-layer organic photovoltaic cell. *Appl. Phys. Lett.* **1986**, *48*, 183–185.
8. Peumans, P.; Uchida, S.; Forrest, S.R. Efficient bulk heterojuction photovoltaic cells using small-molecular-weight organic thin films. *Nature* **2003**, *425*, 158–159.
9. Hiramoto, M.; Fujiwara, H.; Yokoyama, M. Three-layered organic solar cell with a photoactive interlayer of codeposited pigments. *Appl. Phys. Lett.* **1991**, *58*, 1062–1064.

10. Wöhrle, D.; Kreienhoop, L.; Schnurpfeil, G.; Elbe, J.; Tennigkeit, B.; Hiller, S.; Schlettwein, D. Investigation of n/p-junction photovoltaic cells of perylenetetraacarboxylic acid diimides and phthalocyanines. *J. Mater. Chem.* **1995**, *5*, 1819–1829.
11. Loi, M.A.; Denk, P.; Hoppe, H.; Neugebauer, H.; Winder, C.; Meissner, D.; Brabec, C.; Sariciftci, N.S.; Gouloumis, A.; Vázquez, P.; Torres, T. Long-lived photoinduced charge separation for solar cell applications in phthalocyanine-fulleropyrrolidine dyad thin films. *J. Mater. Chem.* **2003**, *13*, 700–704.
12. de la Escosura, A.; Martínez-Díaz, M.V.; Torres, T.; Grubbs, R.H.; Guldi, D.M.; Neugebauer, H.; Winder, C.; Drees, M.; Sariciftci, N.S. New donor-acceptor materials based on random polynorbornenes bearing pendant phthalocyanine and fullerene units. *Chem. Asian. J.* **2006**, *1–2*, 148–154.
13. Ito, O.; D'Souza, F. Recent advances in photoinduced electron transfer processes of fullerene-based molecular assemblies and nanocomposites. *Molecules* **2012**, *17*, 5816–5835.
14. López-Duarte, I.; Wang, M.; Humphry-Baker, R.; Ince, M.; Martínez-Díaz, M.V.; Nazzeeruddin, M.K.; Torres, T.; Grätzel, M. Molecular engineering of zinc phthalocyanines with phosphinic acid anchoring groups. *Angew. Chem. Int. Ed.* **2011**, *50*, 1–5.
15. O'Regan, B.C.; López-Duarte, I.; Martínez-Díaz, M.V.; Forneli, A.; Albero, J.; Morandeira, A.; Palomares, E.; Torres, T.; Durrant, J.R. Catalysis of recombination and its limitation on open circuit voltage for dye sensitized photovoltaic cells using phthalocyanine dyes. *J. Am. Chem. Soc.* **2008**, *130*, 2906–2907.
16. Imahori, H.; Umeyama, T.; Ito, S. Large π-aromatic molecules as potential sensitizers for highly efficient dye-sensitized solar cells. *Acc. Chem. Res.* **2009**, *42*, 1809–1818.
17. He, J.; Benko, G.; Korodi, F.; Polívka, T.; Lomoth, R.; Åkermark, B.; Sun, L.; Hagfeldt, A.; Sundström, V. Modified phthalocyanines for efficient near-IR sensitization of nanostructured TiO_2 electrode. *J. Am. Chem. Soc.* **2002**, *124*, 4922–4932.
18. Clifford, J.N.; Palomares, E.; Nazeeruddin, M.K.; Grätzel, M.; Nelson, J.; Li, X.; Long, N.J.; Durrant, J.R. Molecular control of recombination dynamics in dye-sensitized nanocrystalline TiO_2 films: Free energy *vs*. distance dependence. *J. Am. Chem. Soc.* **2004**, *126*, 5225–5233.
19. de la Torre, G.; Claessens, C.G.; Torres, T. Phthalocyanines: Old dyes, new materials. Putting color in nanotechnology. *Chem. Commun*. **2007**, 2000–2015.
20. Morandeira, A.; López-Duarte, I.; Martínez-Díaz, M.V.; O'Regan, B.; Shuttle, C.; Haji-Zainulabidin, N.A.; Torres, T.; Palomares, E.; Durrant, J.R. Slow electron injection on Ru-phthalocyanine sensitized TiO_2. *J. Am. Chem. Soc.* **2007**, *129*, 9250–9251.
21. Takanabe, K.; Kamata, K.; Wang, X.; Antonietti, M.; Kubota, J.; Domen, K. Photocatalytic hydrogen evolution on dye-sensitized mesoporous carbon nitride photocatalyst with magnesium phthalocyanine. *Phys. Chem. Chem. Phys.* **2010**, *12*, 13020–13025.
22. Chen, F.; Deng, Z.; Li, X.; Zhang, J.; Zhao, J. Visible light detoxification by 2,9,16,23-tetracarboxyl phthalocyanine copper modified amorphous titania. *Chem. Phys. Lett.* **2005**, *415*, 85–88.
23. Shang, J.; Chai, M.; Zhu, Y. Photocatalytic degradation of polystyrene plastic under fluorescent light. *Environ. Sci. Technol.* **2003**, *37*, 4494–4499.

24. Abe, T.; Nagai, K.; Kabutomori, S.; Kaneko, M.; Tajiri, A.; Norimatsu, T. An organic photoelectrode working in the water phase: Visible-light-induced dixoygen evolution by a perylene derivative/cobalt phthalocyanine bilayer. *Angew. Chem. Int. Ed.* **2006**, *45*, 2778–2781.
25. Abe, T.; Tobinai, S.; Taira, N.; Chiba, J.; Itoh, T.; Nagai, K. Molecular hydrogen evolution by organic p/n bilayer film of phthalocyanine/fullerene in the entire visible-light energy region. *J. Phys. Chem. C* **2011**, *115*, 7701–7705.
26. Nagai, K.; Abe, K.; Kaneyasu, Y.; Yasuda, Y.; Kimishima, I.; Iyoda, T.; Imaya, H. A Full-spectrum visible-light-responsive organophotocatalyst film for removal of trimethylamine. *ChemSusChem* **2011**, *4*, 727–730.
27. Zhang, S.; Sakai, R.; Abe, T.; Iyoda, T.; Norimatsu, T.; Nagai, K. Photoelectrochemical and photocatalytic properties of biphasic organic p- and n-type semiconductor nanoparticles fabricated by a reprecipitation process. *ACS Appl. Mater. Interfaces* **2011**, *3*, 1902–1909.
28. Zhang, S.; Arunachalam, P.; Abe, T.; Iyoda, T.; Nagai, T. Photocatalytic decomposition of *N*-methyl-2-pyrrolidone, aldhydes, and thiol by bisphase and p/n junction-like organic semiconductor composite nanoparticles responsive to nearly full spectrum of visible light. *J. Photochem. Photobiol. A* **2012**, *244*, 18–23.
29. Nagai, K.; Morishita, K.; Yoshida, H.; Norimatsu, T.; Miyanaga, N.; Izawa, Y.; Yamanaka, T. Photo-reflection and laser-ablation properties of phthalocyanine/perylene derivative bilayer. *Synth. Met.* **2001**, *121*, 1445–1446.
30. Nagai, K.; Yoshida, H.; Norimatsu, T.; Miyanaga, N.; Izawa, Y.; Yamanaka, T. Uniform laser ablation via photovoltaic effect of phthalocyanine/perylene derivative. *Appl. Surf. Sci.* **2002**, *197–198*, 808–813.
31. Fujishima, A.; Honda, K. Electrochemical photolysis of water at a semiconductor electrode. *Nature* **1972**, *238*, 37–38.
32. O'Regan, B.; Grätzel, M. A low-cost, high-efficiency solar cell based on dye-sensitized colloidal TiO_2 films. *Nature* **1991**, *353*, 737–740.
33. Abe, T.; Nagai, K.; Kaneko, M.; Okubo, T.; Sekimoto, K.; Tajiri, A.; Norimatsu, T. A novel and efficient system of a visible-light-responsive organic photoelectrocatalyst working in a water phase. *ChemPhysChem* **2004**, *5*, 716–720.
34. Abe, T.; Miyakushi, S.; Nagai, K.; Norimatsu, T. Study of the factors affecting the photoelectrode characteristics of a perylene/phthalocyanine bilayer working in the water phase. *Phys. Chem. Chem. Phys.* **2008**, *10*, 1562–1568.
35. Abe, T.; Nagai, K.; Sekimoto, K.; Tajiri, A.; Norimatsu, T. Novel characteristics at a fullerene/water interface in an organic bilayer photoelectrode of phthalocyanine/fullerene. *Electrochem. Commun.* **2005**, *7*, 1129–1132.
36. Abe, T.; Nagai, K.; Ichinohe, H.; Shibata, T.; Tajiri, A.; Norimatsu, T. An efficient oxidation at photofunctional interface of phthalocyanine in combination with fullerene. *J. Electroanal. Chem.* **2007**, *599*, 65–71.
37. Carpenter, M.K.; Corrigan, D.A. Photoelectrochemistry of nickel hydroxide thin films. *J. Electrochem. Soc.* **1989**, *136*, 1022–1026.
38. Abe, T.; Kaneko, M. Reduction catalysis by metal complex confined in a polymer matrix. *Prog. Polym. Sci.* **2003**, *28*, 1441–1448.

39. Sobbi, A.K.; Wöhrle, D.; Schlettwein, D. Photochemical stability of various porphyrins in solution and as thin film electrodes. *J. Chem. Soc. Perkin Trans. 2* **1993**, 481–488.
40. Karmann, E.; Schlettwein, D.; Jaeger, N.I. Photoelectrochemical oxidation of 2-mercaptoethanol at the surface of octacyanophthalocyanine thin film electrodes. *J. Electroanal. Chem.* **1996**, *405*, 149–158.
41. Abe, T.; Ichinohe, H.; Kakuta, S.; Nagai, K. Organic photoanode of fullerene/phthalocyanine working in the water phase with respect to preparation methods of the bilayer film. *Jpn. J. Appl. Phys.* **2010**, *49*, 015101.
42. Haufler, R.E.; Conceicao, J.; Chibante, L.P.F.; Chai, Y.; Byrne, N.E.; Flanagan, S.; Haley, M.M.; O'Brien, S.C.; Pan, C.; Xiao, Z.; *et al*. Efficient production of C60 (buckminsterfullerene), C60H36, and the solvated buckide ion. *J. Phys. Chem.* **1990**, *94*, 8634–8636.

Sample Availability: Samples of the nanoparticles are available from the authors based on the Material Transfer Agreement with Tokyo Institute of Technology (http://ime.res.titech.ac.jp/syusyoku.html).